J Fluoresc (2011) 21:1813–1823
DOI 10.1007/s10895-011-0876-5

ORIGINAL PAPER

An Intramolecular Charge Transfer Fluorescent Probe: Synthesis, Structure and Selective Fluorescent Sensing of Cu^{+2}

Jayaraman Jayabharathi · Venugopal Thanikachalam · Natesan Srinivasan · Karunamoorthy Jayamorthy · Marimuthu Venkatesh Perumal

Received: 9 October 2010 / Accepted: 23 February 2011 / Published online: 24 March 2011
© Springer Science+Business Media, LLC 2011

Abstract A series of substituted imidazoles have been synthesized in very good yield under solvent free condition by grinding 1,2-diketone, aromatic aldehyde and ammonium acetate in the presence of molecular iodine as the catalyst. The short reaction time, good yield and easy workup make this protocol practically and economically attractive and characterized by NMR spectra, X-ray, mass and CHN analysis. An excited state intramolecular proton transfer (ESIPT) process in hydroxy imidazoles (dpip and dptip) have been studied using emission spectroscopy and it was detected that the two distinct ground state rotamers are responsible for the normal and the tautomer emissions. DFT calculations on energy, dipole moment, charge distribution of the rotamers in the ground and excited states of the imidazole derivatives were performed and discussed. DFT analysis about HOMO, HOMO-1, LUMO and LUMO + 1 were carried out and discussed. PES calculation indicates that the energy barrier for the interconversion of two rotamers is too high in the excited state than the ground state.

Keywords NMR · X-ray · ESIPT · PES · CIS

Introduction

Excited state intramolecular proton transfer (ESIPT) phenomena have been investigated in the past decades due to the practical applications of ESIPT exhibiting molecules as laser dyes, photostabilizers, fluorescent probes in biology and light-emitting materials for electroluminescent devices [1–3]. ESIPT typically occurs in aromatic molecules having a phenolic hydroxy group with an intramolecular hydrogen bond to the nearby hetero atom (distance <2 Å) of the same chromophore to form the excited state tautomer. The two distinct intramolecular hydrogen bonded rotamers I and II (Fig. 1) have been detected experimentally in the ground state [4] by the typical ESIPT exhibiting 2-(2′-hydroxyphenyl)benzazole derivatives. Among the two rotamers only enol rotamer II undergoes ESIPT to form the excited state ketotautomer III, which transmits a long wavelength emission while rotamer I is responsible for the short wavelength normal emission. Then the excited keto tautomer luminesce, undergoing a transition to the ground state, the reverse proton transfer takes place and the molecule returns to the enol form (Fig. 1).

Organic solvents are high on the list of damaging chemicals, in recent years solid-state organic reactions have caused great interest. Designing of "green" experimental protocol is an enormous challenge to chemists to improve the quality of the environment for present and future generations. Compounds with an imidazole ring system have many pharmacological properties [5, 6]. Though there are several methods reported [7] in the literature for the synthesis of imidazoles, they suffer from one or more disadvantages such as harsh reaction conditions, poor yields, prolonged time period, use of hazardous and often expensive acid catalysts. Recently, molecular iodine [8] received considerable attention as an inexpensive, nontoxic, readily available catalyst for various organic transformations, affording the corresponding products in excellent yields with high selectivity. Owing to numerous advantages

J. Jayabharathi (✉) · V. Thanikachalam · N. Srinivasan · K. Jayamorthy · M. V. Perumal
Department of Chemistry, Annamalai University, Annamalainagar 608 002 Tamilnadu, India
e-mail: jtchalam2005@yahoo.co.in

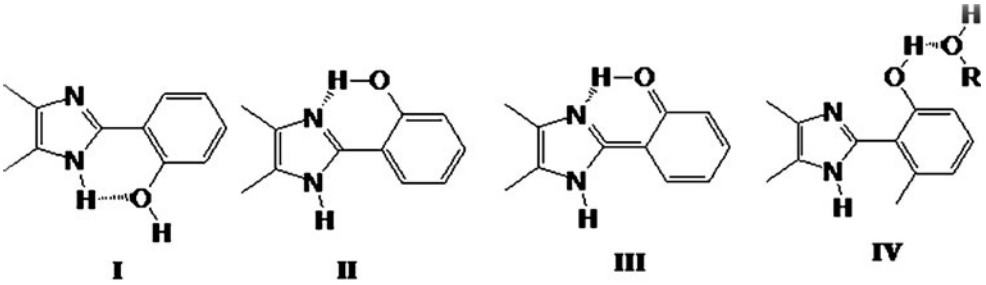

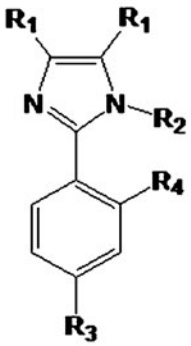

Compounds	R_1	R_2	R_3	R_4
1	CH_3	p-$C_6H_4CH_3$	F	H
2	C_6H_5	C_6H_5	F	H
3	C_6H_5	H	H	OH
4	C_6H_5	p-$C_6H_4CH_3$	H	OH
5	C_6H_5	p-$C_6H_4CH_3$	H	OCH_3
6	C_6H_5	p-$C_6H_4CH_3$	OH	H

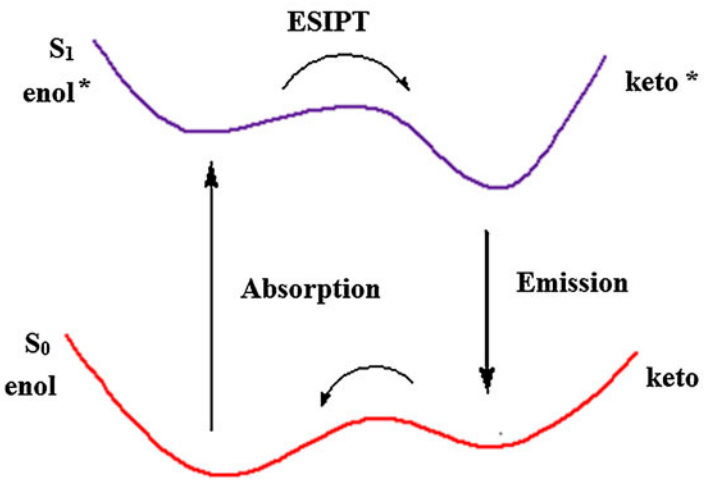

Fig. 1 Rotameric forms of dpip **(3)** and dptip **(4)**

associated with this eco-friendly element, iodine has been explored as a powerful catalyst for various organic transformations [9]. During the course of our studies towards the development of new route to the synthesis of biologically active heterocycles, we wish to report a simple and an efficient method for the synthesis of substituted imidazoles.

In continuation of our previous work, we will focus the light on the photophysical studies of 2-aryl imidazole derivatives (**1**–**6**) synthesized under green experimental condition, ESIPT process of hydroxy imidazoles [dpip(**3**) and dptip (**4**)] and Density Functional Theory (DFT) calculations [10] on energy, dipole moment of various species, HOMO, HOMO-1, LUMO and LUMO + 1 energies and PES studies were performed and discussed.

Experimental

Optical Measurements and Composition Analysis

NMR spectra were recorded for the 2-aryl imidazole derivatives (**1**–**6**) on a Bruker 400 MHz. The ultraviolet–visible (UV–Vis) spectra were measured on UV–Vis spectrophotometer (Perkin Elmer, Lambda 35) and cor-

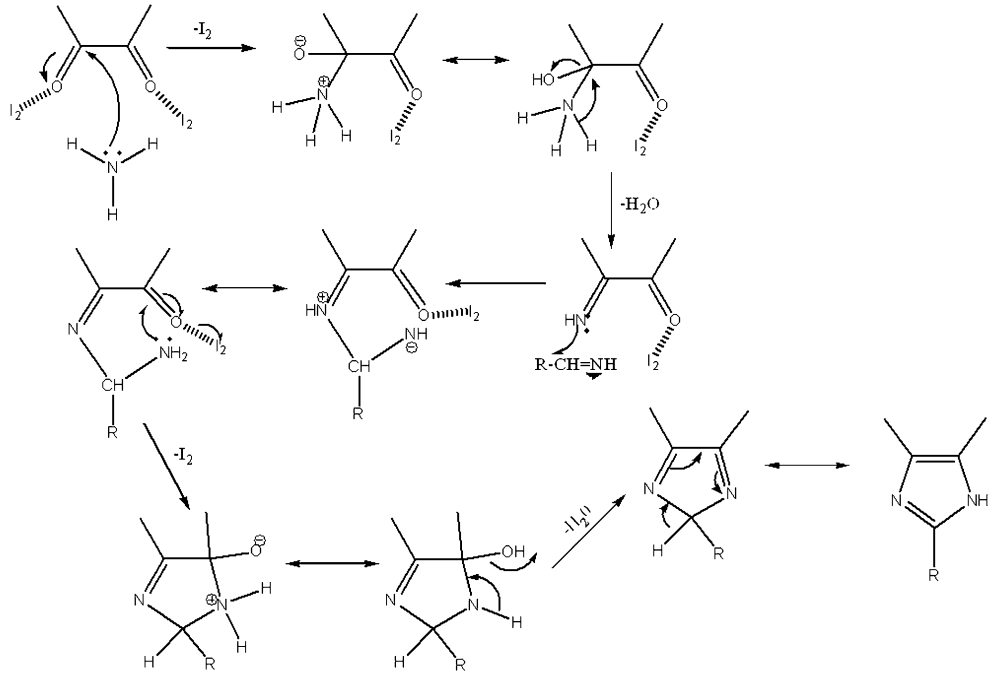

Scheme 1 Mechanism for imidazole formation

rected for background due to solvent absorption. Photoluminescence (PL) spectra were recorded on a (Perkin Elmer LS55) fluorescence spectrometer. Solvents used for spectral measurements are spectroscopic grade. The fluorescence quantum yield were measured in acetonitrile using coumarin 47 as a standard [11] according to the equation, $\Phi_{unk} = \Phi_{std}\left(\frac{I_{unk}}{I_{std}}\right)\left(\frac{A_{std}}{A_{unk}}\right)\left(\frac{\eta_{unk}}{\eta_{std}}\right)^2$ Where, Φ_{unk}, Φ_{std}, I_{unk}, I_{std}, A_{unk}, Φ_{unk} and Φ_{std} are the fluorescence quantum yields, the integration of the emission intensities, the absorbances at the excitation wavelength and the refractive indexes of the corresponding solution of the 2-aryl imidazole derivatives (**1**–**6**) and the standard, respectively. The radiative (k_r) [$k_r = \Phi_p/\tau$] and non-radiative (k_{nr}) [$k_{nr} = 1/\tau - \Phi_p/\tau$] rate constants were calculated using the life time (τ) of the excited state. Mass spectra were recorded on a Varian Saturn 2200 GCMS spectrometer.

General Procedure for the Synthesis of 2-aryl Imidazole Derivatives **(1–6)**

A mixture of aldehyde (1 mmol), benzil (1 mmol), ammonium acetate (2.5 mmol) and iodine (15 mol%) were grined in a mortar at room temperature for appropriate time. The reaction was monitored by TLC and the reaction mixture was treated with aqueous $Na_2S_2O_3$, the formed crude was purified by column chromatography (n-hexane:ethyl acetate (9:1) (Scheme 1). The improved yield of these imidazole derivatives were compared with conventional [12] yields and it is given in parenthesis.

2-(4-fluorophenyl)-4,5-dimethyl-1-p-tolyl-1H-imidazole (fpdmti) (**1**)

Yield: 50%. (30%), mp 130 °C, Anal. calcd. for $C_{18}H_{17}FN_2$: C, 77.12; H, 6.11; N, 9.99. Found: C, 77.00; H, 5.98; N, 9.03. FTIR (cm^{-1}) 1519,1598, 1647, 2364, 2855, 2916, 3540, 3751. ^{1}H NMR (400 MHz, $CDCl_3$): δ 2.01 (s, 3H), 2.29 (s, 3H), 2.43 (s, 3H), 6.87–7.34 (aromatic protons). ^{13}C (100 MHz, $CDCl_3$): δ 9.53, 12.69, 21.18, 114.92, 115.10, 125.44, 127.16, 129.89, 130.20, 133.35, 135.13, 138.57, 144.28, 161.26, 163.23. MS: m/z 280.00, calcd. 280.14.

2-(4-fluorophenyl)-1,4,5-triphenyl-1H-imidazole (fpdpti) (**2**)

Yield: 60%. (32%), mp 242 °C, Anal. calcd. for $C_{27}H_{19}FN_2$: C, 83.05; H, 4.90; N, 7.17. Found: C, 82.00;

Table 1 Photophysical spectral parameters of 2-arylimidazole derivatives (**1**–**6**) in dioxane

Compound	$\lambda_{abs\ (nm)}$	$\lambda_{exi\ (nm)}$	$\lambda_{flu\ (nm)}$
fpdmti (1)	290.5 (303.9)	290.0 (303.0)	362.0 (359.7)
fpdpti (2)	327.0 (316.5)	328.0 (315.1)	386.2 (382.4)
dpip (3)	330.1 (320.1)	332.8 (318.5)	455.1, 496.3 (sh) (430.7)
dptip (4)	340.7 (380.1)	341.7 (381.9)	475.0, 508.0 (sh) (453.0)
mpdpti (5)	313.5 (392.7)	315.0 (396.0)	440.0 (452.1)
dptimp (6)	338.2 (320.1)	340.0 (326.2)	388.2 (385.3)

Values in the parenthesis are recorded in ethanol

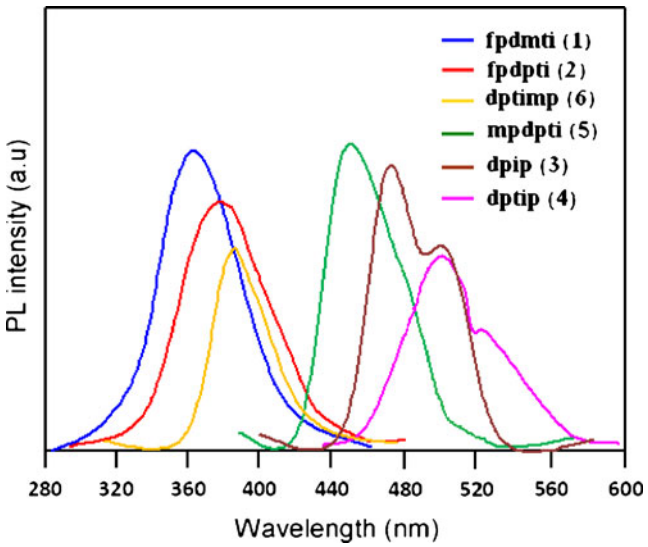

Fig. 2 Emission spectra of 2-aryl imidazole derivatives **1**–**6** in dioxane

H, 5.00; N, 4.78. FTIR (cm^{-1}) 1256, 1645, 2434, 2990, 3456. ^{1}H NMR (400 MHz, $CDCl_3$): δ 6.92 (d, 2H), 7.49–7.80(m,15H), 7.90 (d,2H)(aromatic protons). ^{13}C (100 MHz, $CDCl_3$): δ 126.55, 127.38, 128.10, 128.38, 128.93, 130.69, 131.12, 134. 46, 137.14, 138.29, 146.91. MS: m/z 390.00, calcd. 390.45.

2-(4,5-diphenyl-1H-imidazol-2-yl)phenol(dpip) **(3)**

Yield: 62%. (35%), mp 215 °C, Anal. calcd. for $C_{21}H_{16}N_2O$: C, 80.75; H, 5.16; N, 8.97. Found: C, 79.12; H, 5.20; N, 7.64. FTIR (cm^{-1}) 1640, 2462, 3008, 3462, 3658. ^{1}H NMR (400 MHz, $CDCl_3$): δ 6.93–6.99(m,7H), 7.26–7.52(m,7H), 8.04 (s,1H),12.97(brs,1H) (aromatic protons), ^{13}C (100 MHz, $CDCl_3$): δ 113.36,117.29, 119.32, 125.42,129.09, 130.54, 146.33, 157.17 MS: m/z 312.00, calcd. 312.36.

2-(4,5-diphenyl-1-p-tolyl-1H-imidazol-2-yl)phenol (dptip) **(4)**

Yield: 65%. (36%), mp 215 °C, Anal. calcd. for $C_{28}H_{22}N_2O$: C, 83.56; H, 5.51; N, 6.96. Found: C, 83.00; H, 5.20; N, 6.02. FTIR (cm^{-1}) 1638, 2465, 2996, 3456, 3598. ^{1}H NMR (400 MHz, $CDCl_3$): δ 2.27 (s, 3H), 6.80 (d, 2H), 7.84 (d,2H), 7.16–7.25(m,7H), 7.45–7.51 (m,6H), 9.31 (s,1H),12.50(brs,1H) (aromatic protons), ^{13}C (100 MHz, $CDCl_3$): δ 9.53, 114.73, 120.80, 126.06, 126.33, 127.15, 127.40, 145.87, 157.08. MS: m/z 402.00, calcd. 402.17.

Table 2 Electron density of atoms N(5) and O for dpip (**4**) and dptip (**5**)

Compound	Atom	II	II*	III
(dpip) (4)	N(5)	−0.401	−0.448	0.382
	O	−0.545	−0.528	−0.568
dptip (5)	N(5)	−0.517	−0.589	0.502
	O	−0.640	−0.603	−0.656

Table 3 Relative energies (eV) and dipole moments (D) in the ground and excited state for rotamers I, II and III

Compound	Rotamers	Ground state		Excited state	
		μ (D)	E(eV)	E(eV)	μ(D)
dpip (3)	I	4.51	0.04 (0.00)	4.01 (3.50)	8.65
	II	4.06	0.08 (0.03)	4.56 (3.92)	8.10
	III	5.89	0.58 (0.32)	3.62 (3.08)	4.02
dptip (4)	I	3.82	0.01 (0.00)	4.25 (4.10)	7.46
	II	3.25	0.04 (0.02)	3.82 (3.50)	7.98
	III	4.89	0.42 (0.28)	3.61 (3.10)	3.18

Relative energies are calculated with respect to the ground state minimum energy form in ethanol. Values in the parenthesis are recorded in ethanol

2-(2-methoxyphenyl)-4,5-diphenyl-1-p-tolyl-1H-imidazole (mpdpti) **(5)**

Yield: 62%.(35%), mp 235 °C, Anal. calcd. for $C_{29}H_{24}N_2O$: C, 83.63; H, 5.81; N, 6.73. Found: C, 82.98; H, 5.01; N6.01. FTIR (cm^{-1})1230, 1450, 1605, 2924, 3512,3614. ^{1}H NMR (400 MHz, $CDCl_3$): δ 2.20 (s, 3H), 3.80 (s, 3H),2.40 (s, 3H), 6.77 (d, 2H), 7.05–7.50 (m, 14H), 8.03 (s,2H) (aromatic protons). ^{13}C (100 MHz, $CDCl_3$): δ 9.53, 55.1 115.25, 125.05, 126.47, 127.50, 127.69, 128.68, 129.69 130.45, 145.61. MS: m/z 416.00, calcd. 416.19.

4-(4,5-diphenyl-1-p-tolyl-1H-imidazol-2-yl)phenol (dptimp) **(6)**

Yield: 58%. (30%), mp 231 °C, Anal. calcd. for $C_{28}H_{22}N_2O$: C, 83.56; H, 5.51; N, 6.96. Found: C, 82.58; H, 5.23; N 6.56. FTIR (cm^{-1})12450, 15420, 1635, 2876, 3589, 3721. ^{1}H NMR (400 MHz, $CDCl_3$): δ 2.20 (s, 3H), 6.93 (d, 2H), 7.53–7.89 (m, 14H), 7.92 (d,2H), 12.52 (brs,1H) (aromatic protons). ^{13}C (100 MHz, $CDCl_3$): δ 9.52, 113.20, 119.76, 125.01, 127.50, 127.69, 144.78, 130.45, 158.30 MS: m/z 402.00, calcd. 402.70.

Table 4 Percentage of enol and keto isomeric forms of **3** and **4**

Compound	Ground state		Excited state	
	% enol	% keto	% enol	% keto
dpip(**3**)	100	0	6.5×10^{-16}	100
dptip(**4**)	100	0	1×10^{-274}	100

Results and Discussion

The absorption spectra of 2-aryl imidazole derivatives (**1**–**6**) were almost in coincidence with the excitation spectra, the fluorescent properties were taken for discussion (Table 1). The steric effect from aromatic species at C(2) position has been evaluated in imidazole system, and the steric interaction from the C(2) position has a direct impact on

Table 5 Selected bond lengths (Å), Bond angles (°) and torsional angles (°) of fdpti (**2**)

Bond lengths (Å)	Experimental XRD (Å)	Bond angles (°)	Experimental XRD (º)	Torsional angles (°)	Experimental XRD (º)
N1-C2	1.3798(1.4141)	C2-N1-C5	107.30(106.9283)	C5-N1-C2-N3	−0.64(−0.72)
N1-C5	1.3905(1.4066)	C2-N1-C11	125.41(127.0122)	C5-N1-C2-C21	−179.79(−179.81)
N1-C11	1.4370(1.4159)	C5-N1-C11	127.07(126.0441)	C12-C11-C16-C15	−2.50(−4.01)
N3-C2	1.3194(1.3573)	C2-N3-C4	106.26(106.5784)	C11-C12-C13-C14	0.7(0.8)
N3-C4	1.3798(1.3986)	N1-C2-N3	110.82(110.7521)	C12-C13-C14-C15	−0.80(−0.92)
C2-C21	1.4718(1.4637)	N1-C2-C21	125.85(124.5399)	C13-C14-C15-C16	−0.80(−0.94)
C4-C5	1.3759(1.4204)	N3-C2-C21	123.32(124.7077)	C14-C15-C16-C11	2.4(3.1)
C4-C41	1.4761(1.4539)	N3-C4-C5	110.51(109.7608)	C2-C21-C22-C23	−179.20(−180.42)
C5-C51	1.4785(1.4529)	N3-C4-C41	118.29(122.5708)	C26- C21-C22-C23	−1.36(−1.51)
C11-C12	1.3771(1.4103)	C5-C4-C41	131.20(127.6622)	C2- C21-C26-C25	178.74(180.02)
C11-C16	1.3793(1.4102)	N1-C5-C4	105.11(105.9798)	C22- C21-C26-C25	0.78 (0.82)
C12-C13	1.3810(1.391)	N1-C5-C51	122.73(124.1276)	C21- C22-C23-C24	0.66(0.89)
C13-C14	1.3780(1.3993)	C4-C5-C51	132.12(129.8899)	C22- C23-C24-F4	−178.45(−180.08)
C14-C15	1.3720(1.3992)	N1-C11-C12	119.53(120.448)	C22- C23-C24-C25	0.7(0.92)
C15-C16	1.3825(1.3912)	N1-C11-C16	119.13(120.4048)	F4- C24-C25-C26	177.87(180.12)
C21-C22	1.3897(1.4001)	C12-C11-C16	121.26(119.12)	C23-C24-C25-C26	−1.3(−1.9)
C21-C26	1.3887(1.4024)	C11-C12-C13	119.27(120.0061)	C24-C25-C26-C21	0.5 (0.8)
C22-C23	1.3834(1.3906)	C12-C13-C14	119.78(120.9015)	C4-C41-C42-C43	177.03(179.20)
C23-C24	1.3621(1.4072)	C13-C14-C15	120.59(119.0368)	N3-C2-C21-C22	142.10(144.65)
C24-C25	1.3630(1.3906)	C14-C15-C16	120.18(120.9003)	N3-C2-C21-C26	−35.75(−36.48)
C25-C26	1.3843(1.3916)	C11-C16-C15	118.87(102.0073)	N3-C4-C5-N1	−0.57(0.72)
C41-C42	1.3950(1.4018)	C2-C21-C22	123.50(121.109)	N3-C4-C5-C51	−178.31(−180.16)
C42-C43	1.3755(1.3923)	C2-C21-C26	117.88(119.0524)	C41-C4-C5-N1	−179.56(−180.89)
C43-C44	1.3740(1.3912)	C22-C21-C26	118.59(120.48)	C41-C4-C5-C51	2.7(2.9)
F4-C24	1.3626(1.3541)	C21-C22-C23	120.38(119.4749)	N3-C4-C41-C42	−31.76(−32.83)
C44-C45	1.3650(1.4805)	C22-C23-C24	118.91(120.25)	N3-C4-C41-C46	145.60(147.82)
C45-C46	1.3822(1.3929)	C23-C24-C25	122.85(119.59)	C5-C4-C41-C42	147.16(149.86)
C51-C52	1.3859(1.4022)	C24-C25-C26	118.04(120.3539)	C5-C4-C41-C46	−35.48(−37.21)
C51-C56	1.3960(1.4202)	C21-C26-C25	121.21(120.4815)	N1-C5-C51-C52	135.85(139.17)
C52-C53	1.3860(1.3992)	F4-C24-C23	118.56(119.85)	N1-C5-C51-C56	−45.92(−47.83)
C53-C54	1.3780(1.3902)	F4-C24-C25	118.58(119.92)	C4-C5-C51-C52	−46.76(47.71)
C54-C55	1.3670(1.3912)	C23-C24-C25	122.85(123.12)	C4-C5-C51-C56	131.48(133.33)
C55-C56	1.3779(1.3886)	C24-C25-C26	118.04(120.16)	N1-C11-C12-C13	−175.70(−176.20)
		C4-C41-C42	118.31(120.56)	C46-C41-C42-C43	−0.48(−0.59)
		C4-C41-C46	123.79(125.23)	C4-C41-C46-C45	−177.52(−179.82)
		C42-C41-C46	117.86(119.21)	C42-C41-C46-C45	−0.15(−0.18)
		C41-C42-C43	120.84(122.12)	C42-C43-C44-C45	−0.2(−0.4)
		C42-C43-C44	120.44(122.98)	C5-C51-C52-C53	177.49(179.70)
		C43-C44-C45	119.41(121.86)	C56-C51-C52-C53	−0.79(−0.92)
		C5-C51-C52	120.62(121.92)	C51-C52-C53-C54	0.4(0.6)
		C5-C51-C56	121.15(122.03)	C52-C53-C54-C55	0.3(0.5)

Values in the paranthesis are theoretically calculated

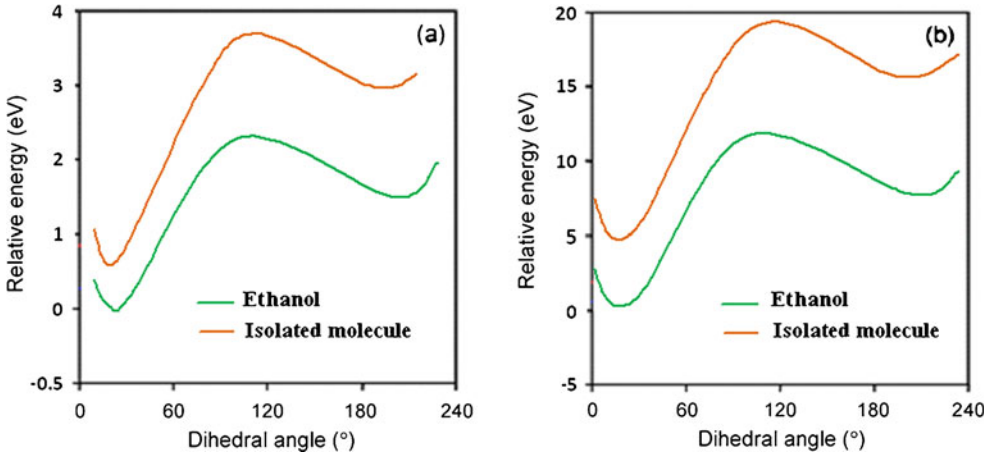

Fig. 3 **a** PES for the interconversion of the rotamers of dptip **(3)** in the ground state. **b** PES for the interconversion of the rotamers of dptip **(4)** in the ground state

the fluorescent properties. The emission properties of fluorophores **1**–**6** were examined in dioxane and ethanol and they possess strong fluorescence property with quantum yields ranging from 0.42–0.78.

The hydroxy substituted 2-aryl imidazoles [dpip (**3**) and dptip (**4**)] in aprotic solvents exists as two different intramolecular hydrogen bonded isomers I and II and excitation of the isomer II should lead to the formation of the keto isomer III due to ESIPT (Fig. 1), while excitation of the isomer I must yield the normal emission. But, we found out that the fluorescence spectra of dpip (**3**) and dptip (**4**) in dioxane contain one emission band at shorter wavelength and one small shoulder peak at higher wavelength which reveal that only the isomer II of these molecules were stable under these conditions.

However, in the case of hydroxyl containing solvent (EtOH), a short wavelength emission band appears for dpip (**3**) and dptip (**4**) and this observation is absent in the fluorescence spectra of **1, 2, 5** and **6** (Fig. 2). This result can be explained by the presence of intermolecular hydrogen bonding with solvent molecule (EtOH) leading to the stabilization of solvated isomer IV in which ESIPT is impossible [13].

In order to support the ESIPT mechanism in dpip (**3**) and dptip(**4**), we calculated the electron density for the keto and enol isomers of the dpip (**3**) and dptip(**4**) by DFT in both the ground and the excited states (Table 2), which reveal that excitation of enol isomer leads to an increase in the electron density at N (5) atom and decrease at O atom resulting in ESIPT and formation of the excited keto isomer in excited state. Then, the excited keto isomer emits luminescence and returns to the ground state keto form, which is characterized by a large positive charge at N (5) atom and negative charge at O atom. As a result, a reverse process occurs in the ground state of the molecule producing an initial molecule in the enol form.

Correlation Between Intramolecular Hydrogen Bonding and ESIPT Process

The existence of intramolecular hydrogen bond in dpip (**3**) and dptip(**4**) is confirmed by the presence of the singlet at 12.97 ppm (dpip) and 12.50 ppm (dptip) in the ^{1}H NMR spectra which is a typical signal for hydrogen bonded hydrogen atom. In order to reveal the contribution of the intramolecular hydrogen bonding to their optical properties, the fluorescence spectra of dpdip (**4**) and its derivative mpdpti (**5**) were measured in dioxane solvent under identical condition (Fig. 2). A dual fluorescence was detected for dptip (**4**) with emission peak centered at 475 and 508 nm respectively. The emission peak at shorter wavelength at 475 nm is assigned to rotamer I and longer wavelength band at 508 nm is assigned to rotamer II [3]

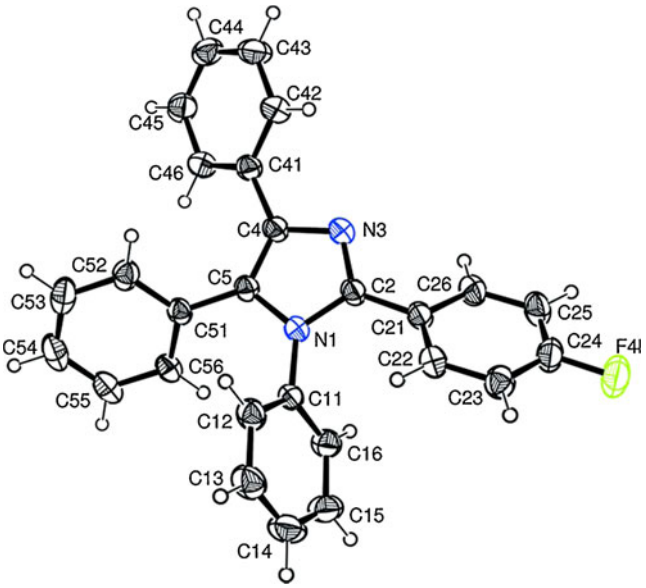

Fig. 4 ORTEP diagram of fdpti**(2)**

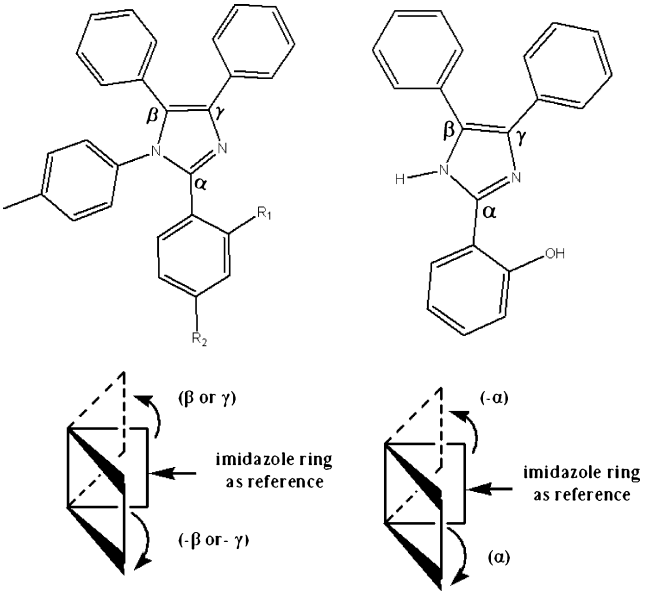

Fig. 5 α, β and γ twists in imidazole derivatives

whereas mpdpti (**5**) exhibits emission peak only at 440 nm, absence of additional peak at longer wavelength confirms the absence of intramolecular hydrogen bond in mpdpti (**5**) which further evident that in dptip (**4**) intramolecular hydrogen bond is the essential driving force for ESIPT.

ESIPT Energy Barrier Calculation

The ESIPT phenomenon has inspired a large number of theoretical calculations [14–17]. The ground state geometries of the three species, I, II, and III for both dpip (**3**) and dptip(**4**) were optimized using the DFT/6-311G (d,p) method for exploring the ESIPT mechanism. Complete optimization of all geometrical parameters gives the ground state energy of each species. The energy of the excited state was calculated using the standard CIS method. The energies and dipole moment of the species I, II, and III in the ground and excited states are given in Tables 3 and 4 whereas the electron density for the keto and enol isomers of the dpip

Table 6 Deviation parameters (°) of imidazole from other rings

Compound	(α)	(β)	(γ)
1	−43.68	5.03	−179.02
2	42.16	−2.12	−178.87
3	−21.90	1.49	−179.22
4	−89.62	−5.08	−179.03
5	−139.70	−2.12	−178.88
6	42.16	−2.12	−178.87

Table 7 Quantum yield and thermodynamic parameters of imidazole derivatives **1–6**

Compound	ϕ_f	τ_f (ns)	k_r (ns^{-1})	k_{nr} (ns^{-1})	HOMO (a.u)	LUMO (a.u)	Eg (a.u)
fpdmti (**1**)	0.71	1.42	0.50	0.20	−0.2999	−0.183	0.117
fpdpti (**2**)	0.60	1.44	0.42	0.27	−0.305	−0.196	0.109
dptip (**3**)	0.78	1.61	0.48	0.14	−0.302	−0.200	0.102
dptip (**4**)	0.42	1.72	0.24	0.34	−0.304	−0.002	0.302
mpdpti (**5**)	0.39	1.35	0.29	0.45	−0.306	−0.196	0.110
dptimp (**6**)	0.60	1.40	0.42	0.29	−0.307	−0.196	0.111

(**3**) and dptip(**4**) in the ground and the excited states are listed in Table 5. In the excited state the nitrogen atom becomes richer in electron density than the hydroxylic oxygen atom. This redistribution of the π-electron densities in the excited electronic state is the driving force for the intramolecular proton transfer from the hydroxylic group to the nitrogen atom. The potential energy (PE) curves (Fig. 3a and b) for the interconversion of isomers I and II of dptip (**5**) in the ground and the excited states reveal that for isolated dptip (**5**) in the ground state, the barrier for interconversion is 2.5 kcal/mol and 1.4 kcal/mol in ethanol. In the excited state the barrier for dmtip (**5**) in the isolated molecule and in the alcohol medium are 10.6 and 7.9 kcal/mol, respectively. The barriers for interconversion in the excited state are much higher than that in the ground state. From the relative heat of formation of enol and keto isomers, the percentage of enol and keto isomers of dpip (**3**) and dptip (**4**) are calculated (Tables 3 and 4). The calculated results reveal that the existence of 100% enol isomer in the ground state and 100% keto isomer in the excited state, supported the experimental results.

Table 8 Absorption and fluorescence spectral data of Co^{2+}, Hg^{2+}, Cu^{2+}, and Pb^{2+} chelates in acetonitrile

Compound	Chemisensor	λ_{em} (nm)
dptip (3)	3	430.7
	3+Cu^{2+}	440.0
	3+Hg^{2+}	490.2
	3+Pb^{2+}	442.1
	3+Co^{2+}	443.7
dptip (4)	4	453.0
	4+Cu^{2+}	462.1
	4+Hg^{2+}	501.5
	4+Pb^{2+}	465.2
	4+Co^{2+}	462.7

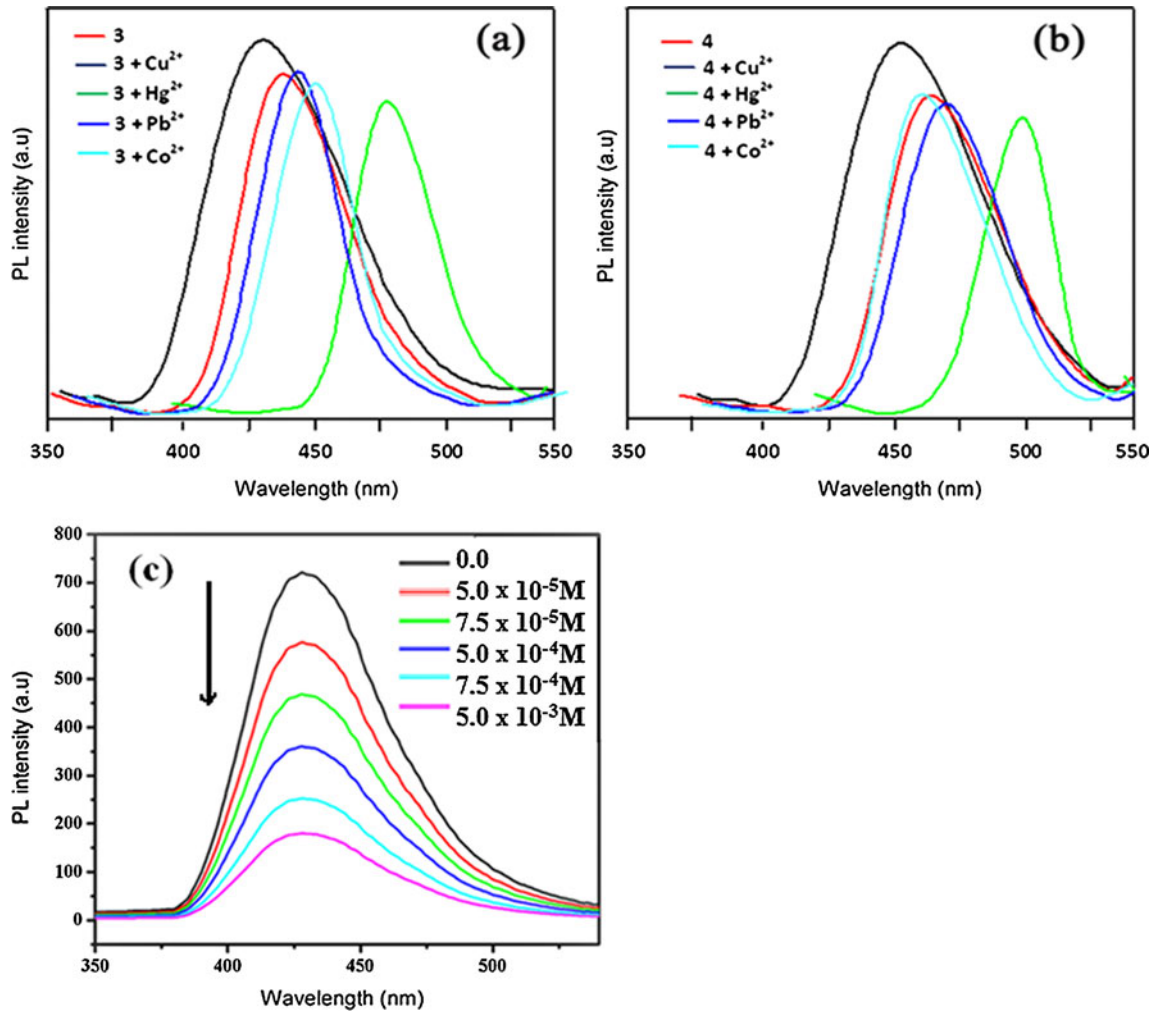

Fig. 6 Fluorescence spectra of dpip **(3)** and dptip **(4)** in the presence of various metal ions

X-ray Analysis: Crystal Structure

X-ray data of fdpti (**2**) (Table 5) reveal that the imidazole ring is essentially planar and makes the dihedral angles of 62.80°, 36.98°, 33.16° and 46.24° respectively, with the substituent rings in the C1, C2, C4 and C5 positions. The two phenyl groups at C(4) and C(5) positions of the imidazole ring are twisted from each other by 51.10° The individual twist from the imidazole is 33.10° (for phenyl at the 4-position) and 46.24° [for phenyl at C(5)] respectively (Fig. 4). In order to eliminate crystal packing effect in the solid state, the molecular geometry of **1**–**6** is further examined by DFT calculation [DFT/B3LYP16-31G(d,p)] [10] to make necessary comparison on an equal state basis. Three key twists, designated as α, β, and γ have been examined. α is used to indicate the twist of imidazole ring from the aromatic six-membered ring at C(2), β and γ are used for twists of imidazole ring from phenyls at C(5) and C(4) positions respectively (Fig. 5). By comparison of results in Table 6, several additional interesting structural features can be concluded that the γ twist is always smaller than the β twist. the β twist originates from the interaction of substituent at N(1) of the imidazole with the phenyl at C (5) whereas the γ twist is a result of chain interaction event, triggered by the interaction of the phenyl at C(4) with the other one at C(5). The β twist always increases upon the substitution at N(1) of the imidazole derivatives compared to the parent counterparts and the substitution increases the β twist but decreases the γ twist. The present structural

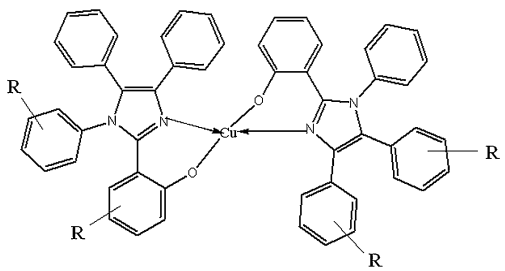

Fig. 7 Chelate structure of (Cu^{+2}-Ligand)

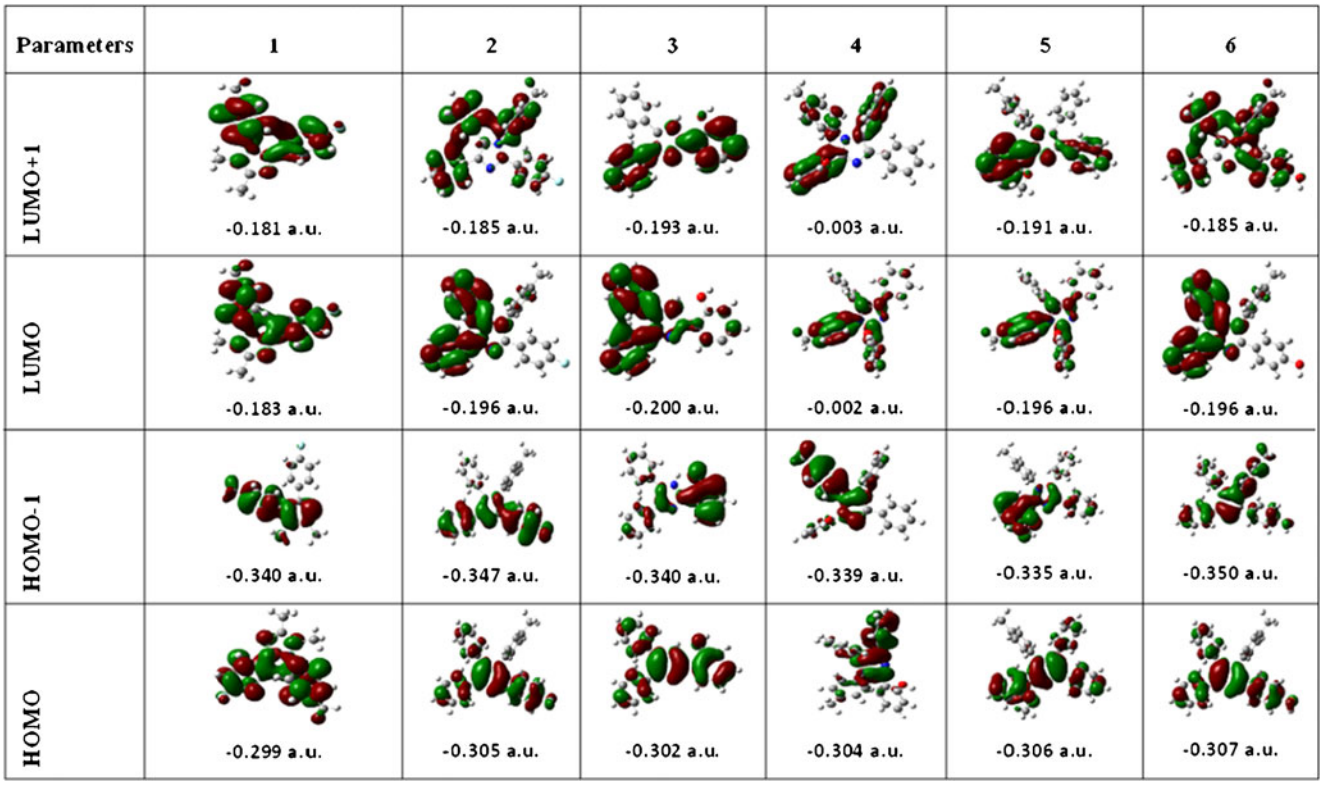

Fig. 8 HOMO-1, HOMO, LUMO and LUMO + 1 orbital picture of (**1**–**6**)

information allows us to further explore the correlation between structural features and fluorescent property. It reveals that α twist is correlated with fluorescent property, the larger the α twist, the more drop the fluorescence quantum yield. Such a clear correlation indicates the importance of coplanarity between imidazole and the aromatic ring at C(2). This correlation can be ascribed to the conjugation rigidity. When the two adjacent aromatic species are in a coplanar geometry, the p-orbitals from the C–C bond connecting the two species will have maximal overlapping and the two rings will have a rigid and delocalized conjugation, as the result, the bond is no longer a pure single bond, as evident from the X-ray data of fdpti (**2**). The present bond distance of C2–C6 is 1.454(4)Å (Table 5) is shorter than the regular single bond distance between two sp2 carbon's (1.48 Å) [17], because of delocalization. When the two rings are deviated from each other, the p-orbital overlapping will be reduced. The partial conjugation will lead to less rigid structure, therefore, radiationless twist motion will deactivate the emitting state, leading to the low quantum yields (Table 7). Thus, it is suggested that fluorophores with the substitution at C(2) with a minimum loss of fluorescence property. Optimization of **1**–**6** have been performed by DFT at B3LYP/6-311G (d,p) using Gaussian-03 and the selected bond angles of fdpti (**2**) are given in Table 5 and compared with XRD data. All these XRD data are in good agreement with the theoretical values. However, from the theoretical values it can be found that most of the optimized bond lengths, bond angles and dihedral angles are slightly higher than that of XRD values. These deviations can be attributed to the fact that the theoretical calculations were aimed at the isolated

Table 9 The calculated electronic transitions of **1** and **3**

Compound	Transition	Molecular orbital contribution	E (eV)	λ_{max} (nm)	Oscillator strength (f)
fpdmti**(1)**	$S_O \rightarrow S_1$	HOMO → LUMO HOMO-1 → LUMO	5.1853	291.11	0.023
dpip**(3)**	$S_O \rightarrow S_2$	HOMO → LUMO + 1	6.9926	177.3	0.0029
	$S_O \rightarrow S_1$	HOMO-1 → LUMO	5.978	331.8	0.9341
	$S_O \rightarrow S_2$	HOMO → LUMO + 1	6.6664	185.98	0.8143

molecule in the gaseous phase whereas the XRD results were aimed at the molecule in the solid state.

Selective Fluorescent Sensing of Cu^{2+}

The observed non-radiative emission of these fluorophores may be due to n−π* transition [18]. Imidazole derivatives have been used to construct highly sensitive fluorescent chemisensors for sensing and imaging of metal ions and its chelates with Ir^{3+} are the major components for organic light emitting diodes [19, 20] and are promising candidates for fluorescent chemisensor for metal ions, if their radiationless channel could be blocked by metal binding. In the presence of transition metal ions such as Co^{2+}, Hg^{2+}, Pb^{2+} and Cu^{2+} an enhancement of fluorescent intensity was observed to a different extent (Table 8) which shows that the metal ions binding, blocks the radiationless decay channel in dpip (**3**) and dptip (**4**) (Fig. 6). The radiative (k_r) and non-radiative (k_{nr}) rate constants were calculated for **3** and **4** in Cu^{2+} in acetonitrile and found that the substantial increase in the quantum yield in the presence of Cu^{2+} is due to dramatic decrease in nonradiative transition whereas the radiative constant remains unchanged within the experimental error. This means that the radiationless decay in dpip (**3**) and dptip (**4**) is blocked upon metal binding (Fig. 7) and the emission of chelate (Cu^{2+} -ligand) orginates only from π−π * state [18].

Electronic Properties

The frontier orbitals (HOMO and LUMO) determined the way in which the molecule interacts with other species. The frontier orbital gap (Table 6) helps to characterize the chemical reactivity and kinetic stability of the molecule. A molecule with a small frontier orbital gap is more polarizable and is generally associated with high chemical reactivity, low kinetic stability and is also termed as soft molecule [21]. The HOMO is the orbital that primarily acts as an electron donor and the LUMO is the orbital that largely acts as the electron acceptor. The 3D plots of the frontier orbitals HOMO and LUMO of **1**–**6** is shown in Fig. 8. It can be seen from the figures the HOMO is located on the phenyl ring attached to the carbon of the imidazole derivative and the unfilled π* orbital (LUMO) located on the imidazole ring. The HOMO → LUMO transition implies that intramolecular charge transfer takes place [22–24] within the molecule. Therefore, introduction of an electron donating substituent into the phenyl ring attached to the nitrogen raises the energy of the LUMO resulting in a blue-shift of the emission. On the other hand, the introduction of the electron donating substituent into the aldehydic phenyl ring raises the energy of the HOMO, leading to the red shift of the emission [22–24]. The calculated energy gap explains the eventual charge transfer interactions within the molecule. The optimized HOMO-1, HOMO, LUMO and LUMO +1 molecular orbitals of **1**–**6** revels that HOMO-1 and HOMO have identical nodal patterns i.e., nodal between the phenyl and imidazole ring portions of the orbital. Therefore the π interaction between two rings is anti-bonding in character. The S_1 has a contribution from HOMO → LUMO, HOMO-1 → LUMO. The vertical excitation energy from the ground state to the $S_1(\pi-\pi^*)$ was calculated which remarkable agreement with the corresponding experimental results. $S_1 \rightarrow S_o$ transitions involves HOMO → LUMO + 1 molecular orbitals (Table 9).

Conclusion

Intermolecular hydrogen bonding of dpip (**3**) and dptip(**4**) with water giving rise to IV impede the ESIPT process, resulting in an increase in the quantum yield of normal emission at the expense of the tautomer emission. However, the intermolecular hydrogen bonding with alcohol is not strong enough to compete with the intramolecular hydrogen bonding in hydroxy substituted imidazole derivatives. Hence, tautomer emission dominates over normal emission in alcohol at room temperature. In the presence of transition metal ions such as Co^{2+}, Hg^{2+},Pb^{2+} and Cu^{2+} an enhancement of fluorescent intensity was observed to a different extent which shows that the metal ions binding, blocks the radiationless decay channel in dpip (**3**) and dptip (**4**) so that the imidazoles are promising candidates for fluorescent chemisensors. The HOMO → LUMO transition implies that intramolecular charge transfer takes place within the molecule.

Acknowledgment One of the author Dr. J. Jayabharathi, Associate professor in Chemistry, Annamalai University is thankful to Department of Science and Technology [No. SR/S1/IC-07/2007] and University Grants commission (F. No. 36-21/2008 (SR)) for providing fund to this research work.

References

1. Qian Y, Li S, Zhang G, Wang Q, Wang S, Xu H, Li C, Li Y, Yang G (2007) Aggregation-induced emission enhancement of 2-(2′-Hydroxyphenyl)benzothiazole-based excited-state intramolecular proton-transfer compounds. J Phys Chem A 111:5861–5868
2. Rodembusch FS, Leusin FP, Campo LF, Stefani V (2007) Excited state intramolecular proton transfer in amino 2-(2'-hydroxyphenyl)benzazole derivatives: effects of the solvent and the amino group position. J Lumin 126:728–734
3. Wu Y, Peng X, Fan J, Gao S, Tian M, Zhao J, Sun S (2007) Fluorescence sensing of anions based on inhibition of excited-state intramolecular proton transfer. J Org Chem 72:62–66

4. Das K, Sarkar N, Ghosh AK, Majumdar D, Nath DN, Bhattacharyya K (1994) Excited state intramolecular proton transfer in 2-(2'-hydroxyphenyl) benzimidazole and -benzoxazole: effect of rotamerism and hydrogen-bonding. J Phys Chem 98:9126–9132
5. Lambardino JG, Wiseman EH (1974) Preparation and antiinflammatory activity of some nonacidic trisubstituted imidazoles. J Med Chem 17:1182–1188
6. Maier T, Schmierer R, Bauer K, Bieringer H, Buerstell H, Sachse B (1989) US Patent 820335, 1989. Chem Abstr 111:19494
7. Lantos I, Zhang W, Shiu X, Eggleston DS (1993) Synthesis of imidazoles via hetero-cope rearrangements. J Org Chem 58:7092–7095
8. Parveen A, Ahmed MD, Shaikh KA, Deshmukh SP, Pawar RP (2007) Efficient synthesis of 2,4,5-triaryl substituted imidazoles under solvent free conditions at room temperature. Arkivoc xvi:12–18
9. Jianwei S, Dong Y, Cao L, Wang X, Wang S, Hu YY (2004) Highly efficient chemoselective deprotection of O, O-Acetals and O, O-Ketals catalyzed by molecular iodine in acetone. J Org Chem 69:8932–8934
10. Frisch MJ, Trucks GW, Schlegel HB, Scuseria GE, Robb MA, Cheeseman JR, Montgomery JA, Vreven T Jr, Kudin KN, Burant JC, Millam JM, Iyengar SS, Tomasi J, Barone V, Mennucci B, Cossi M, Scalmani G, Rega N, Petersson GA, Nakatsuji H, Hada M, Ehara M, Toyota K, Fukuda R, Hasegawa J, Ishida M, Nakajima T, Honda Y, Kitao O, Nakai H, Klene M, Li X, Knox JE, Hratchian P, Cross JB, Adamo C, Jaramillo J, Gomperts R, Stratmann RE, Yazyev O, Austin AJ, Cammi R, Pomelli C, Ochterski JW, Ayala PY, Morokuma K, Voth GA, Salvador P, Dannenberg JJ, Zakrzewski VG, Dapprich S, Daniels AD, Strain MC, Farkas O, Malick DK, Rabuck AD, Raghavachari K, Foresman JB, Ortiz JV, Cui Q, Baboul AG, Clifford S, Cioslowski J, Stefanov BB, Liu G, Liashenko A, Piskorz P, Komaromi I, Martin RL, Fox DJ, Keith T, Al-Laham MA, Peng CY, Nanayakkara A, Challacombe M, Gill PMW, Johnson B, Chen W, Wong MW, Gonzalez C, Pople JA (2004) Gaussian 03, Revision C.02, Gaussian, Inc.: Wallingford, CT
11. Saravanan K, Srinivasan N, Thanikachalam V, Jayabharathi J (2011) Synthesis and photophysics of some novel imidazole derivatives used as sensitive fluorescent chemisensors. J Fluoresc 21:65–80
12. Jayabharathi J, Thanikachalam V, Srinivasan N, Saravanan K (2010) Synthesis, structure, luminescent and Intramolecular proton transfer in some imidazole derivatives. J Fluoresc. doi:10.1007/s10895-010-0747-5
13. Barbara PF, Walsh PK, Brus LE (1989) Picosecond kinetic and vibrationally resolved spectroscopic studies of intramolecular excited-state hydrogen atom transfer. J Phys Chem 93:29–34
14. Feng K, Hsu FL, Veer DVD, Bota K, Bu XR (2004) Tuning fluorescence properties of imidazole derivatives with thiophene and thiazole. J Photochem Photobiol A Chem 165:223–228
15. Woolfe GJ, Melzig M, Schneider S, Dörr F (1983) The role of tautomeric and rotameric species in the photophysics of 2-(2′-hydroxyphenyl) benzoxazole. Chem Phys 77:213–221
16. Sobolewski AL (1993) The mechanism of excited-state hydrogen transfer in 2-hydroxypyridine. Chem Phys Lett 211:293–299
17. Dogra SK (2005) Excited-state inter- and intramolecular proton transfer inmethyl 3-hydroxy-2-quinoxalinate: effects of solvent and acid or base concentrations. J Lumin 114:101–117
18. Zhou Z, Fahrni CJ (2004) A fluorogenic probe for the copper(I)-catalyzed azide-alkyne ligation reaction: modulation of the fluorescence emission via 3(n, π^*)−1(π, π^*) inversion. J Am Chem Soc 126:8862–8863
19. Huang WS, Lin JT, Chien CH, Tao YT, Sun SS, Wen YS (2004) Highly phosphorescent Bis-cyclometalated Iridium complexes containing Benzimidazole-Based ligands. Chem Mater 16:2480–2488
20. Chen CH, Shi J (1998) Metal chelates as emitting materials for organic electroluminescence. Coord Chem Rev 171:161–174
21. Fleming I (1976) Frontier orbitals and organic chemical reactions. Wiley, NewYork, p 5
22. Padmaja L, Ravikumar C, Sajan D, Hubert Joe I, Jayakumar VS, Pettit GR, Faurskov Neilsen O (2009) Density functional study on the structural conformations and intramolecular charge transfer from the vibrational spectra of the anticancer drug combretastatin-A2. J Raman Spectrosc 40:419–428
23. Ravikumar C, Hubert Joe I, Jayakumar VS (2008) Charge transfer interactions and nonlinear optical properties of push-pull chromophore benzaldehyde phenylhydrazone: a vibrational approach. Chem Phys Lett 460:552–558
24. Fukui K, Yonezawa T, Shingu H (1952) A molecular orbital theory of reactivity in aromatic hydrocarbons. J Chem Phys 20:722–725